# A long noncoding RNA regulates inflammation resolution by mouse macrophages through fatty acid oxidation activation

Yukiteru Nakayama[a], Katsuhito Fujiu[a], Ryuzaburo Yuki[b,c], Yumiko Oishi[c], Masaki Suimye Morioka[a], Takayuki Isagawa[d], Jun Matsuda[a], Tsukasa Oshima[a], Takumi Matsubara[a], Junichi Sugita[a], Fujimi Kudo[b], Atsushi Kaneda[e], Yusuke Endo[f,g], Toshinori Nakayama[f], Ryozo Nagai[h], Issei Komuro[a], and Ichiro Manabe[b,1]

[a]Department of Cardiovascular Medicine, Graduate School of Medicine, University of Tokyo, Bunkyo-ku, 113-8654 Tokyo, Japan; [b]Department of Disease Biology and Molecular Medicine, Graduate School of Medicine, Chiba University, Chuo-Ku, 260-8670 Chiba, Japan; [c]Department of Biochemistry & Molecular Biology, Nippon Medical School, Bunkyo-ku, 113-8602 Tokyo, Japan; [d]Data Science Center, Jichi Medical University, Shimotsuke-shi, 392-0498 Tochigi, Japan; [e]Department of Molecular Oncology, Graduate School of Medicine, Chiba University, Chuo-ku, 260-8670 Chiba, Japan; [f]Department of Immunology, Graduate School of Medicine, Chiba University and AMED-CREST, AMED, Chuo-ku, 260-8670 Chiba, Japan; [g]Laboratory of Medical Omics Research, Kazusa DNA Research Institute, Kisarazu, 292-0818 Chiba, Japan; and [h]Jichi Medical University, Shimotsuke-shi, 392-0498 Tochigi, Japan

Edited by Christopher K. Glass, University of California San Diego, La Jolla, CA, and approved May 11, 2020 (received for review April 2, 2020)

**Proper resolution of inflammation is vital for repair and restoration of homeostasis after tissue damage, and its dysregulation underlies various noncommunicable diseases, such as cardiovascular and metabolic diseases. Macrophages play diverse roles throughout initial inflammation, its resolution, and tissue repair. Differential metabolic reprogramming is reportedly required for induction and support of the various macrophage activation states. Here we show that a long noncoding RNA (lncRNA), *lncFAO*, contributes to inflammation resolution and tissue repair in mice by promoting fatty acid oxidation (FAO) in macrophages. *lncFAO* is induced late after lipopolysaccharide (LPS) stimulation of cultured macrophages and in Ly6C$^{hi}$ monocyte-derived macrophages in damaged tissue during the resolution and reparative phases. We found that *lncFAO* directly interacts with the HADHB subunit of mitochondrial trifunctional protein and activates FAO. *lncFAO* deletion impairs resolution of inflammation related to endotoxic shock and delays resolution of inflammation and tissue repair in a skin wound. These results demonstrate that by tuning mitochondrial metabolism, *lncFAO* acts as a node of immunometabolic control in macrophages during the resolution and repair phases of inflammation.**

Long noncoding RNA | macrophage | inflammation

Macrophages recognize molecules associated with pathogens and cell damage via pattern recognition receptors, such as Toll-like receptors (TLRs), which activate stimulus-regulated transcription factors, including NF-κB (1, 2). For example, TLR4 recognizes lipopolysaccharide (LPS) and activates an NF-κB–driven program of proinflammatory gene expression. In this way, macrophages play a key role as a first-line defense against pathogens and tissue damage. However, the actions of macrophages are not limited to this early response. They also play diverse and crucial roles in the resolution of inflammation, repair of tissue, and restoration of homeostasis. For example, early after tissue damage, proinflammatory activated macrophages promote acute inflammation, which is essential for elimination of cell debris and pathogens (3). After this early phase, inflammation subsides in coordination with activation of the repair phase. During this phase transition, macrophages change their phenotypes and play critical roles in inflammation resolution and tissue repair. Dysregulation of this phenotypic transition in macrophages prolongs inflammation and impedes tissue repair, which may underlie various chronic inflammatory diseases, including cardiovascular disease (4, 5). Accordingly, the activation states of macrophages must be tightly regulated (3).

Recent studies have identified cellular metabolism as a novel regulator of macrophage activation states (3, 6). For example, M1 proinflammatory activation is characterized by high glycolytic metabolism, whereas M2 alternative activation induced by IL-4 stimulates oxidative phosphorylation (OXPHOS) (6, 7). Importantly, interfering with that metabolic change impairs macrophage activation and function, demonstrating that metabolic reprogramming is a crucial part of the regulatory programs governing macrophage function and phenotype. Indeed, metabolic pathways and metabolites appear to be intricately linked to the cellular machinery that controls and executes macrophage activities (8).

Long noncoding RNAs (lncRNAs) are defined as RNAs over 200 nucleotides in length without protein-coding potential. It is becoming increasingly clear that lncRNAs are key regulatory mediators in a variety of biological processes. For example, lncRNAs are essential for controlling stemness and cell differentiation (9–12). A number of lncRNAs are also associated with various diseases, including cancer, cardiovascular diseases, and autoimmune diseases (13). Consequently, lncRNAs have attracted broad interest as novel biomarkers and potential therapeutic targets. So far, however, the functions of only a limited number of

## Significance

**Proper resolution of inflammation is essential for restoration of homeostasis. Macrophages are particularly important for this process and dynamically change their functional phenotypes during the transition from inflammatory activation to resolution. we identify a long noncoding RNA, *lncFAO*, that promotes inflammation resolution. Deletion of *lncFAO* perturbed late suppression of inflammatory gene expression after LPS treatment and exacerbated endotoxic shock and skin wounds in vivo, which demonstrates that *lncFAO* is integral to inflammation resolution in macrophages. Mechanistically, *lncFAO* directly interacts with the HADHB subunit of mitochondrial trifunctional protein and activates fatty acid oxidation. Our data indicate that *lncFAO* is a mediator of metabolic reprogramming for resolution of inflammation in macrophages.**

Author contributions: Y.N., K.F., R.N., and I.M. designed research; Y.N., K.F., R.Y., Y.O., M.S.M., J.M., T.O., T.M., J.S., F.K., A.K., Y.E., T.N., and I.M. performed research; Y.N., K.F., Y.O., M.S.M., T.I., I.K., and I.M. analyzed data; and Y.N. and I.M. wrote the paper.

The authors declare no competing interest.

This article is a PNAS Direct Submission.



Data deposition: The data reported in this paper have been deposited in the Gene Expression Omnibus (GEO) database, https://www.ncbi.nlm.nih.gov/geo (accession nos. GSE130056 and GSE129963).

[1]To whom correspondence may be addressed. Email: manabe-tky@umin.ac.jp.

This article contains supporting information online at https://www.pnas.org/lookup/suppl/doi:10.1073/pnas.2005924117/-/DCSupplemental.

First published June 8, 2020.

lncRNAs have been elucidated, although the results highlight the diverse modes of action of lncRNAs, including epigenetic regulation and various posttranscriptional and posttranslational mechanisms (14). Several lncRNAs are reportedly involved in regulating the functions of monocytes and macrophages (15). For example, lincRNA-Cox2, PACER, AS-IL1α, and FIREE are all acutely up-regulated by TLR activation and enhance inflammatory gene expression via transcriptional and posttranscriptional mechanisms (16–20). In contrast, lnc-IL7R, lincRNA-EPS, and Mirt2 suppress the inflammatory function of macrophages (21–23). lncRNAs are thus important regulators of macrophage activation. However, expression of the aforementioned lncRNAs is acutely (<6 h) controlled by LPS; little is known about the function of lncRNAs that respond later (e.g., during the resolution phase).

In the present study, we identified a lncRNA, designated *lncFAO*, that represses proinflammatory activation of macrophages during the late phase of inflammatory responses. We found that *lncFAO* exerts its effects by activating the β-subunit of mitochondrial trifunctional protein (hydroxyacyl-CoA dehydrogenase/3-ketoacyl-CoA thiolase/enoyl-CoA hydratase β-subunit; HADHB), a key enzyme in fatty acid β-oxidation (FAO), which is required for late suppression of proinflammatory cytokines. Within injured tissues, *lncFAO* is expressed in Ly6C$^{hi}$ macrophages during the inflammation resolution and tissue-repair phases. *lncFAO* deletion impairs resolution of inflammation and wound healing. These findings indicate that by controlling metabolic reprogramming, *lncFAO* mediates proper resolution of inflammation and is required for expression of proresolution/reparative phenotypes in macrophages.

## Results

***lncFAO*, a Late-Response Macrophage lncRNA Was Identified.** In the present study we aimed to identify novel lncRNAs that regulate the inflammatory response of macrophages, particularly during the resolution phase (24). Because lncRNA expression is known to be highly diverse among different cell types (25, 26), we sought lncRNAs expressed in bone marrow-derived macrophages (BMDMs) by sequencing polyA$^+$ RNAs. Upon assembling the transcripts (27), we found that LPS-treated BMDMs expressed >1,000 potential lncRNAs. Among them, we focused on lncRNAs whose expression was increased at late times after LPS stimulation (e.g., 24 and 48 h).

We chose 11 of the late-response lncRNAs identified because their expression levels were higher and were sustained for 24 or 48 h after LPS treatment in BMDMs (*SI Appendix*, Table S1*A*) and then assessed the effects of their knockdown on inflammatory gene expression (*SI Appendix*, Fig. S1 and Table S1*B*). Among the candidate lncRNAs, knockdown of a lncRNA designated *lncFAO* significantly increased expression of the proinflammatory genes *Il1b* and *S100a8* in LPS-treated BMDMs (Fig. 1*A* and *SI Appendix*, Fig. S1 *A* and *B*). *lncFAO* was transiently down-regulated 4 h after LPS treatment but was markedly up-regulated 8 h after treatment (Fig. 1*B*). Gene set enrichment analysis (GSEA) of RNA-sequencing (RNA-seq) results showed that the Molecular Signatures Database (MSigDB) hallmark gene sets (28, 29) related to inflammatory responses and NF-κB signaling were up-regulated in *lncFAO* knockdown cells 24 h after LPS treatment (*SI Appendix*, Table S2). These results suggest that *lncFAO* may be important for suppressing LPS-induced inflammatory genes at late times (e.g., 24 h) and may contribute to the resolution of inflammation.

*lncFAO* gene has a multiexonic structure (Fig. 1*C*). According to the widely used coding-potential assessment tools Annocript and CPAT (30, 31), the coding potential of *lncFAO* is low (Annocript noncoding potential score: 0.9653; CPAT coding probability: 0.0839). The transcription start site for *lncFAO* exhibited high H3K4me3 deposition (Fig. 1*C*), which is a hallmark of active promoters of mRNA-coding genes (32). We also found that the promoter, 5′-upstream regions, and an intronic region were all bound by PU.1, which is the macrophage lineage-determining transcription factor, and by NF-κB p65, which is the major signal-dependent transcription factor responding to TLR4 activation (33). Interestingly, after TLR4 activation, p65 binding associated with decreased H3K4me3 and H3K27ac deposition at 4 h (Fig. 1*C*), which reflects promoter and enhancer activity, respectively (34), and suggests NF-κB binding is involved in the transient repression of *lncFAO* transcription. Once expressed, the majority (>70%) of *lncFAO* transcripts were detected in the cytosol (*SI Appendix*, Fig. S1*C*).

Expression of *lncFAO* exhibited a tissue-selective pattern and was undetectable or very low in many tissues in mice under steady-state conditions (*SI Appendix*, Fig. S1*D*). But whereas *lncFAO* RNA was undetectable in normal hearts, its level was very high in the infarcted area 7 d after myocardial infarction (MI), which suggests its strong up-regulation by inflammation (*SI Appendix*, Fig. S1*D*). Whereas Ly6C$^{hi}$ monocyte-derived macrophages initially dominate during the inflammatory phase of MI, during the repair phase (days 3 to 7 post-MI) Ly6C$^{lo}$ macrophages become predominant (35). *lncFAO* was highly expressed in proinflammatory Ly6C$^{hi}$ macrophages in injured hearts, but was undetectable in cardiac-resident macrophages in the steady state (Fig. 1*D* and *SI Appendix*, Fig. S1*E*). As compared to Ly6C$^{hi}$ macrophages during the active inflammatory phase on day 2 after MI, expression of *lncFAO* was increased in Ly6C$^{hi}$ macrophages during the resolution phase on day 8 (36). Moreover, *lncFAO* expression was much higher in Ly6C$^{hi}$ macrophages than in Ly6C$^{lo}$ macrophages on day 8, suggesting that *lncFAO* is up-regulated in Ly6C$^{hi}$ macrophages during the resolution phase after MI.

To further delineate expression of *lncFAO* in MI, we analyzed its expression in a publicly available single-cell RNA-seq dataset (37). Farbehi et al. analyzed single-cell expression profiles of the total cardiac interstitial cells and *Pdgfra*$^+$ fibroblasts in the ventricles on days 3 and 7 post-MI and on day 7 postsham. We found that *lncFAO* expression was confined to the populations of *Ptprc*$^+$ leukocytes (*SI Appendix*, Fig. S2). The majority of *lncFAO*-expressing cells were also *Cd68*$^+$*Itgam*$^+$, indicating that they were monocytes/macrophages.

Analysis of *Cd68*$^+$ macrophage populations showed that *lncFAO* is expressed in *Ly6c2*$^{hi}$*Ccr2*$^{hi}$*Adgre1*$^{int}$ macrophages (cluster 1 in *SI Appendix*, Fig. S2*C*), which appear to correspond to CD11b$^+$F4/80$^+$Ly6C$^{hi}$ macrophages identified with flow cytometry (Fig. 1*D*) in the sham and day 7 post-MI hearts (*SI Appendix*, Fig. S3*A*), and a modest level *lncFAO* expression was also observed in a population of *Ly6c2*$^{int}$*Msr1*$^{hi}$*Arg1*$^+$ macrophages (cluster 2) on day 7 post-MI. *lncFAO* expression was transiently down-regulated on day 3 in cluster 1 cells. On day 7, cluster 1 cells were characterized by relatively high expression of inflammatory cytokines, such as *Il6* and *Il1b*, as well as high expression of *Tgfb1* (*SI Appendix*, Fig. S3*A*). Cluster 1 cells were also marked by higher expression of *Nr4a1*, which has been shown to limit inflammation during the repair phase after MI (*SI Appendix*, Fig. S2*C*) (35). Gene ontology enrichment analyses also showed that the transcriptome of cluster 1 cells was enriched in gene sets related to both inflammation and resolution, including "negative regulation of immune system process" and "wound healing" in *Cd68*$^+$ cells (*SI Appendix*, Fig. S3*B*). GSEA also revealed that OXPHOS is enriched in cluster 1 cells (*SI Appendix*, Fig. S3*C*). The transcriptome of cluster 2 cells was characterized by genes related to cell migration, angiogenesis and wound healing. Cluster 2 cells also expressed relatively high levels of *Il10* (*SI Appendix*, Fig. S3*A*). Collectively, these results show that *lncFAO* is expressed in monocyte-derived *Ly6c2*$^{hi\text{-}int}$ macrophages that appear to contribute to inflammation resolution and tissue repair after MI.

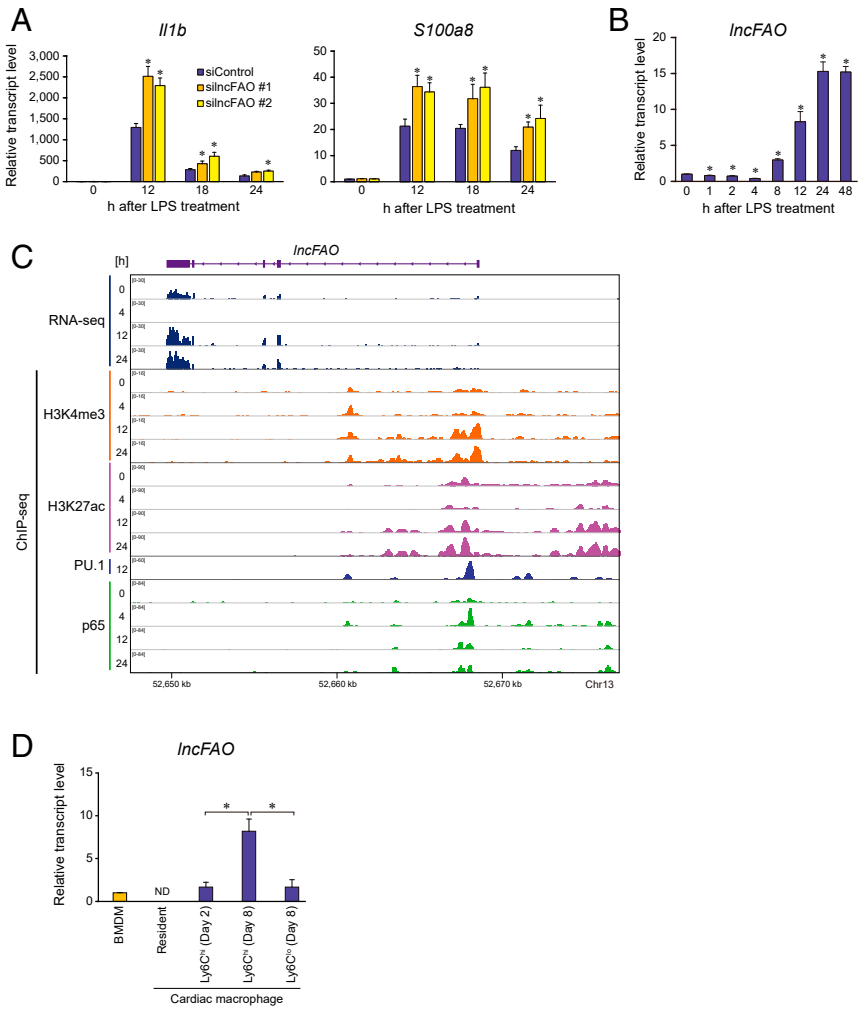


**Fig. 1.** *lncFAO* is induced late after LPS treatment and affects proinflammatory cytokine expression. (*A*) Quantitative PCR analysis of *Il1b* and *S100a8* expression in BMDMs transfected with control (siControl) or two types of siRNA targeting *lncFAO* (silncFAO). Analyses were performed at the indicated times after LPS treatment. mRNA levels were first normalized to those of 18s rRNA and then to the level in untreated control siRNA-transfected BMDMs. $n = 3$. $^*P < 0.05$ vs. control siRNA at the same time point. Tukey–Kramer's post hoc test. (*B*) Levels of *lncFAO* RNA expression in BMDMs treated with LPS. mRNA levels were first normalized to those of 18s rRNA and then to the level in untreated control BMDMs. $n = 3$. $^*P < 0.05$ vs. 0 h in a two-tailed unpaired Student's *t* test. (*C*) Gene locus of *lncFAO*. An IGV Genome Browser shot shows the RNA expression and ChIP-seq results of H3K4me3, H3K27ac, PU.1, and NF-κB p65 in BMDMs at the indicated times after TLR4 activation. (*D*) Levels of *lncFAO* expression in macrophages. Cardiac-resident macrophages ($CD45^+D11b^+F4/80^+Ly6G^-$) were isolated from mice in a steady state. MI was induced by ligating the left anterior descending artery, after which $Ly6C^{hi}$ macrophages ($CD11b^+F4/80^+Ly6C^{hi}Ly6G^-$) and $Ly6C^{lo}$ macrophages ($CD11b^+F4/80^+Ly6C^{lo}Ly6G^-$) were isolated from the infarcted lesions at the indicated times post-MI. $^*P < 0.05$. Tukey–Kramer's post hoc test. ND, not determined.

***lncFAO* Negatively Regulates Inflammatory Activation of Macrophages.** To analyze the function of *lncFAO*, we used CRISPR/Cas9 technology to generate several *lncFAO* knockout ($lncFAO^{-/-}$) mouse lines. One of those lines had a 201-bp deletion with no additional mutations at predicted off-target sites (*SI Appendix*, Fig. S4 *A–C*). These mice were born at a normal Mendelian ratio and grew normally (*SI Appendix*, Fig. S4*D*), with no apparent gross abnormalities. Using qPCR detecting a region spanning exons 3 to 5, we confirmed that *lncFAO* transcripts were largely eliminated in BMDMs from $lncFAO^{-/-}$ mice (KO1 in *SI Appendix*, Fig. S4*E*). *lncFAO* RNA expression was also nearly eliminated in another line of *lncFAO* knockout mice that had a 711-bp deletion (KO2 in *SI Appendix*, Fig. S4 *B* and *E*). Mice from this second line also grew normally, and BMDMs derived from that line exhibited a cytokine gene-expression profile that was similar to that in cells from the KO1 line (*SI Appendix*, Fig. S4*F*). In the following experiments we used the KO1 line.

Transcriptome analysis of $lncFAO^{-/-}$ BMDMs 12 h after LPS treatment indicated increased expression of genes belonging to gene sets related to inflammatory responses (Fig. 2*A*). qPCR analysis showed that *lncFAO* deletion increased levels of *Il1a* and *Il6* expression after LPS treatment (Fig. 2*B*). Secretion of IL-1α and IL-6 was also increased in $lncFAO^{-/-}$ BMDMs (Fig. 2*C*). Conversely, *lncFAO* overexpression decreased IL-1α and IL-6 levels in BMDMs 24 h post-LPS (Fig. 2*D*). Taken together, these results demonstrate that *lncFAO* negatively regulates expression of proinflammatory cytokines, such as IL-1α and IL-6 in response to LPS.

To gain additional insight into the effects of *lncFAO* deletion on BMDM function, we analyzed the transcriptome over the course of LPS stimulation. GSEA showed that the hallmark gene sets "inflammatory response" and "IFN-αi response" were up-regulated in $lncFAO^{-/-}$ cells at all timepoints (*SI Appendix*, Table S3). In untreated cells, gene sets related to "Myc signaling," "angiogenesis," "cell growth," and "metabolism" were up-regulated. These results further confirm that *lncFAO* restricts inflammatory activation of BMDMs. In line with the transcriptome changes,

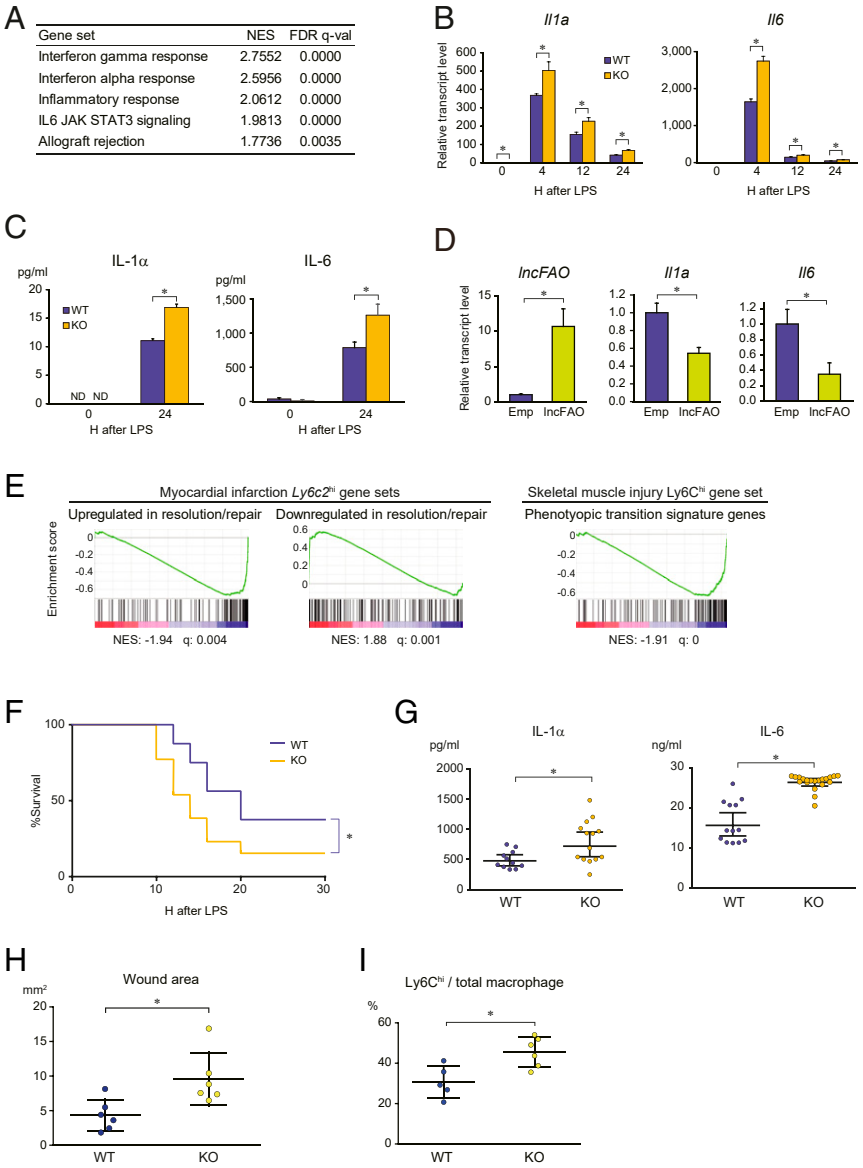


**Fig. 2.** *lncFAO* deletion augments inflammatory responses. (*A*) Transcriptomes of BMDMs from WT and *lncFAO*$^{-/-}$ mice were analyzed using RNA-seq 12 h after LPS treatment. Gene set enrichment was analyzed using GSEA (28). Shown are false-discovery rate < 0.05 MSigDB hallmark gene sets up-regulated in *lncFAO*$^{-/-}$ cells as compared to WT cells. NES, normalized enrichment scores. (*B*) qPCR analysis of *Il1a* and *Il6* in BMDMs from WT and *lncFAO*$^{-/-}$ mice. mRNA levels were first normalized to those of 18s rRNA and then to the level in untreated (0 h) WT BMDMs. $n = 3$ for each group. *$P < 0.05$, two-tailed unpaired Student's *t* test. (*C*) IL-1α and IL-6 levels in medium collected from BMDM cultures 24 h after LPS treatment. $n = 3$. *$P < 0.05$, two-tailed unpaired Student's *t* test. (*D*) BMDMs were transfected with empty vector (*E*) or an *lncFAO* expression vector; 24 h after transfection, the cells were treated with LPS, and mRNA levels were assessed after an additional 24 h. mRNA levels were first normalized to those of 18s rRNA and then to the level in WT BMDMs. $n = 3$. *$P < 0.05$, two-tailed unpaired Student's *t* test. (*E*) Dysregulation of the signature genes representing the transition of Ly6C$^{hi}$ macrophages from the inflammation to resolution/repair phase after MI or skeletal muscle injury in *lncFAO*$^{-/-}$ BMDMs. Shown are GSEA enrichment scores in untreated *lncFAO*$^{-/-}$ BMDMs as compared to WT BMDMs (28). The MI gene sets consist of the genes up-regulated (107 genes) or down-regulated (144 genes) from day 3 to day 7 in *Ly6c2*$^{hi}$ macrophages in the single-cell RNA-seq dataset for MI (*SI Appendix*, Figs. S2 and S3) (37), and the skeletal muscle injury gene set consists of the genes enriched in Ly6C$^{hi}$ macrophages on day 4 in injured skeletal muscle (127 genes) (38). (*F*) Kaplan–Meier survival curves for WT and *lncFAO*$^{-/-}$ mice intraperitoneally injected with a high-dose of LPS (50 μg/mg). $n = 10$ for each group. *$P < 0.05$, log-rank test. (*G*) Mice were intraperitoneally injected with a low-dose of LPS (20 μg/mg), and blood levels of IL-1α and IL-6 were analyzed 12 h after the injection. Shown are concentrations of each mouse and the means ± SD $n = 10$ (WT) or 12 (KO) mice. *$P < 0.05$, two-tailed unpaired Student's *t* test. (*H*) Quantification of the wound area 8 d after skin excision in mice transplanted with WT or *lncFAO*$^{-/-}$ bone marrow. *$P < 0.05$, two-tailed unpaired Student's *t* test. (*I*) Flow cytometric analysis of the phenotypes of the macrophages (CD45.2$^{+}$CD11b$^{+}$F4/80$^{+}$Ly6G$^{-}$) infiltrating the wound area. The fraction of proinflammatory Ly6C$^{hi}$ macrophages is shown. *$P < 0.05$, two-tailed unpaired Student's *t* test.

immunostaining showed that 24 h after LPS treatment nuclear NF-κB levels remained higher in *lncFAO*$^{-/-}$ BMDMs than WT BMDMs (*SI Appendix*, Fig. S5), which supports the notion that *lncFAO* is important for resolution of LPS-induced inflammatory activation.

To assess the function of *lncFAO* within injured tissue, we analyzed the effects of *lncFAO* deletion on the signature genes representing the transcriptomic change from the inflammation to resolution/repair phase in Ly6C$^{hi}$ macrophages (cluster 1 cells) after MI (*SI Appendix*, Fig. S2). We generated gene sets consisting of the genes up-regulated or down-regulated in Ly6C$^{hi}$ macrophages from day 3 to day 7 post-MI. GSEA showed that *lncFAO* deletion dysregulated expression of these genes in

untreated BMDMs (Fig. 2*E* and *SI Appendix*, Table S4). In another well-characterized mouse model, cardiotoxin-mediated skeletal muscle injury, Ly6C$^{hi}$ macrophages markedly alter the phenotype from proinflammation toward proresolution/repair on day 4 after injury (38). We found that the gene signature of Ly6C$^{hi}$ macrophages at the transition period was down-regulated in *lncFAO*$^{-/-}$ BMDMs (Fig. 2*E*). Taken together, these results suggest that *lncFAO* contributes to the acquisition of the phenotypic characteristic to Ly6C$^{hi}$ macrophages during the inflammation resolution and repair phases after tissue injury.

***lncFAO* Is Required for Proper Inflammatory Resolution and Healing.** To gain further insight into the function of *lncFAO* in inflammatory responses in vivo, we used an endotoxic shock model induced by intraperitoneal injection of LPS. In lethal-dose LPS experiments, *lncFAO* knockout reduced survival (Fig. 2*F*). Twelve hours after administration of a sublethal dose of LPS, serum IL-1α and IL-6 levels were significantly higher in *lncFAO*$^{-/-}$ than WT mice (Fig. 2*G*). It appears that *lncFAO* suppresses proinflammatory activation of macrophages, particularly during the late-resolution phase of the LPS response.

We also assessed the contribution of *lncFAO* in hematopoietic cells to inflammatory resolution using a skin wound excision model in mice that had received a bone marrow transplant (BMT) from WT or *lncFAO*$^{-/-}$ mice (WT-BMT and *lncFAO*$^{-/-}$-BMT mice). The wound repair was slower in *lncFAO*$^{-/-}$-BMT than WT-BMT mice (Fig. 2*H* and *SI Appendix*, Fig. S6*A*). In skin excision models, transition from predominantly Ly6C$^{hi}$ proinflammatory monocytes/macrophages to predominantly Ly6C$^{lo}$ macrophages has been shown to occur 2 to 3 d after the wounding (39). In *lncFAO*$^{-/-}$-BMT mice, however, the Ly6C$^{hi}$ cell fraction remained high on day 8 postinjury (Fig. 2*I*). Moreover, infiltration of larger numbers of leukocytes was apparent in the wounds of *lncFAO*$^{-/-}$-BMT mice (*SI Appendix*, Fig. S6*B*). These observations indicate that inflammation persists 8 d after skin excision in *lncFAO*$^{-/-}$-BMT mice and that *lncFAO* in macrophages are important for proper resolution of inflammation and progression to healing.

***lncFAO* Associates with the HADHB Subunit of Mitochondrial Trifunctional Protein.** Although lncRNAs within the nucleus can control gene transcription through a variety of mechanisms (40–42), the major cytosolic localization of *lncFAO* prompted us to hypothesize that it may affect macrophage activation by interacting with cytosolic proteins. To test this idea, we constructed a biotinylated *lncFAO* RNA probe and used it to pull down protein complexes from cytosolic extracts from BMDMs by modifying the chromatin isolation by RNA purification (ChIRP) method to obtain cytosolic RNA–protein complexes (43, 44). Electrophoresis of the pulled down samples revealed a band that showed a higher intensity in samples from LPS-treated cells than from untreated cells or cells treated with an antisense probe (*SI Appendix*, Fig. S7*A*). Mass-spectrometric analysis of the gel band identified HADHB and several other proteins with high sequence coverages (*SI Appendix*, Fig. S7*B*). Because an earlier study showed that HADHB interacts with *Ren* mRNA, indicating its RNA binding capacity (45), we focused on HADHB as a potential interacting partner of *lncFAO*.

With its thiolase activity, HADHB catalyzes the last three steps of FAO to yield an acyl-CoA that is two carbons shorter than the original substrate plus acetyl-CoA (Fig. 3*A*). As expected, HADHB was detected in the precipitates of BMDM lysates using a biotinylated *lncFAO* RNA probe (Fig. 3*B*). That HADHB associates with *lncFAO* was further confirmed when HADHB was detected after using anti-*lncFAO* oligos to pull down endogenous complexes containing *lncFAO* from LPS-treated BMDM lysates (*SI Appendix*, Fig. S8). No HADHB was detected after pull-down using anti-*LacZ* oligos or in samples treated with RNase (Fig. 3*C*), which indicates that the ribonucleoprotein complexes were specifically retrieved by *lncFAO*, not as a result of nonspecific interactions between probe DNAs and HADHB. These data confirm that *lncFAO* associates with HADHB.

***lncFAO* Activates HADHB and FAO.** Because HADHB is localized in mitochondria, we further analyzed the localization of *lncFAO* by separating the mitochondrial fraction from the cytosolic fraction. We found that approximately half of *lncFAO* (~56%) was present in the mitochondrial fraction of BMDMs 24 h after LPS treatment (Fig. 3*D*). FISH of *lncFAO* RNA also showed that the majority of *lncFAO* colocalizes with mitochondrial protein COXIV in BMDMs (*SI Appendix*, Fig. S9).

Mitochondrial levels of both HADHB protein (Fig. 3*E*) and *Hadhb* mRNA (Fig. 3*F*) were decreased by LPS treatment. Interestingly, the LPS-induced decrease in HADHB protein was greater in *lncFAO*$^{-/-}$ BMDMs than in WT cells, although the levels were comparable in untreated cells (Fig. 3*E*). In contrast, the lack of *lncFAO* did not affect *Hadhb* mRNA levels (Fig. 3*F*), which suggests *lncFAO* acts posttranscriptionally to affect mitochondrial HADHB levels after LPS treatment.

Because *lncFAO* in mitochondria binds HADHB, we hypothesized that *lncFAO* may affect HADHB enzymatic activity. To test that idea, we measured the thiolase-catalyzed conversion of acetoacetyl-CoA to acetyl-CoA in BMDM lysates. *lncFAO*$^{-/-}$ lysates exhibited less thiolase activity than WT lysates (Fig. 4*A*). Moreover, addition of *lncFAO* RNA to *lncFAO*$^{-/-}$ lysates enhanced the thiolase activity, while the antisense RNA for *lncFAO* failed to do so. This suggests *lncFAO* activates HADHB enzyme.

Because HADHB is essential for FAO, we used a flux analyzer to test whether *lncFAO* deletion affects cellular metabolism. The basal oxygen consumption rate (OCR) was much lower in *lncFAO*$^{-/-}$ BMDMs than in WT cells (Fig. 4 *B* and *C*). The fraction of the OCR sensitive to etomoxir (48), a carnitine palmitoyltransferase-1 (CPT-1) inhibitor, after addition of carbonyl cyanide-p-trifluoromethoxyphenylhydrazone (FCCP), a mitochondrial OXPHOS uncoupler that induces maximal respiration, was much smaller in *lncFAO*$^{-/-}$ cells than in WT cells (Fig. 4*D*). CPT-1 is the rate-limiting step in the transport of long-chain FAs into mitochondria for oxidation (49). The decrease in etomoxir-sensitive OCR in *lncFAO*$^{-/-}$ cells is thus indicative of reduced FAO capacity.

We also analyzed oxygen consumption in LPS-treated cells using a phosphorescent oxygen probe. Again, oxygen consumption was lower in LPS-treated *lncFAO*$^{-/-}$ cells than WT cells (Fig. 4*E*). In addition, mitochondrial membrane potential was reduced in *lncFAO*$^{-/-}$ cells, suggesting the lack of *lncFAO* impairs mitochondrial function. Taken together, these results show that *lncFAO* is important for mitochondrial FAO and health, acting at least in part through regulation of HADHB.

Finally, we tested whether HADHB dysfunction is responsible for the heightened proinflammatory activation of *lncFAO*$^{-/-}$ BMDMs. When *Hadhb* was knocked down in BMDMs using small-interfering RNA (siRNA), *Il1a* and *Il6* expression was increased in LPS-treated BMDMs (Fig. 4*F* and *SI Appendix*, Fig. S10). Similarly, *Hadhb* knockdown led to increased IL-6 levels in conditioned medium (Fig. 4*G*). These results show that HADHB dysfunction enhances inflammatory activation of macrophages. In contrast, in the *Hadhb* knocked down cells an additional knockdown of *lncFAO* did not alter *Il6* or *Il1a* levels (Fig. 4*F*), supporting the notion that *Hadhb* is required for the regulatory action of *lncFAO*. Moreover, *Hadhb* knockdown did not increase IL-6 levels in conditioned medium of *lncFAO*$^{-/-}$ BMDMs (*SI Appendix*, Fig. S11). These results suggest that *lncFAO* and HADHB work together in the same pathway to regulate the inflammatory activation of macrophages. Taking these data together, we find that *lncFAO* appears to be important for suppression of TLR4-induced proinflammatory cytokine expression

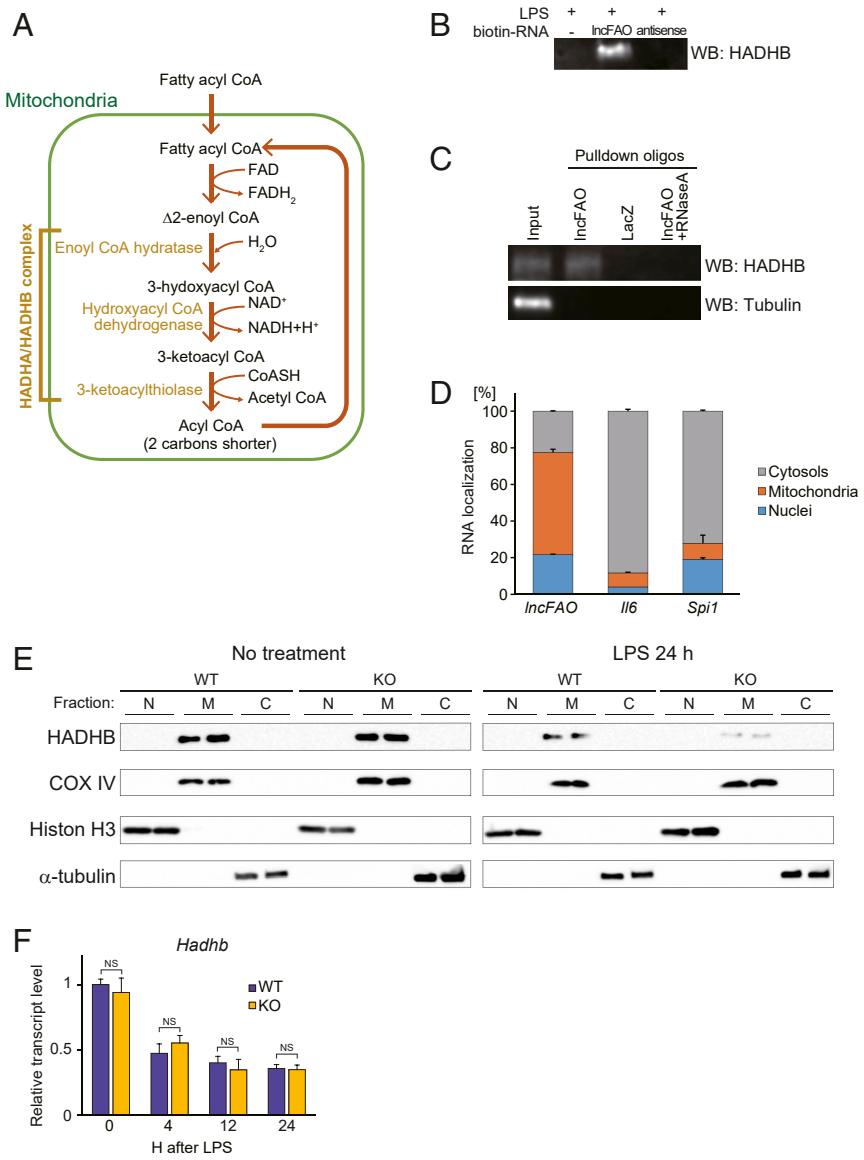


**Fig. 3.** *lncFAO* binds to HADHB and enhances its enzymatic activity. (*A*) Schematic of the FAO pathway. (*B*) Western analysis of HADHB in samples pulled down from BMDM lysates 24 h after LPS treatment. The lysates were pulled down with biotinylated RNA probes for *lncFAO* or its antisense RNA. (*C*) Twenty-four hours after LPS treatment, BMDM lysates were incubated with biotin-conjugated antisense oligonucleotides targeting *lncFAO* and pulled down with streptavidin beads. Oligos against LacZ were used as a control. A RNaseA-treated sample was used an additional control. HADHB and tubulin were analyzed in the pulled down samples using Western blotting. (*D*) Distribution of RNA in the cellular compartments of BMDMs 24 h after LPS treatment. RNA abundances in the three cell subfractions were analyzed using qPCR. $n = 3$. (*E*) Western analysis of the nuclear (N), mitochondrial (M), and nonmitochondrial cytosolic (C) fractions of WT and *lncFAO*$^{-/-}$ BMDMs treated with or without LPS, as indicated. COX IV, Histone H3, and α-tubulin and were detected as internal controls for the mitochondrial, nuclear, and cytosolic fractions, respectively. (*F*) *Hadhb* mRNA levels in WT and *lncFAO*$^{-/-}$ BMDMs at the indicated times after LPS treatment. mRNA levels were first normalized to those of 18s rRNA and then to the level in untreated WT BMDMs. $n = 3$ for each group. NS, not significant in a two-tailed unpaired Student's *t* test.

during the resolution phase, in part by activating FAO through binding to HADHB.

## Discussion

In the present study, we demonstrate that *lncFAO* is expressed in macrophages at late times after LPS treatment and that it suppresses proinflammatory cytokine expression. In LPS-treated BMDMs and Ly6C$^{hi}$ macrophages within injured tissues, *lncFAO* is induced at the resolution phase, which is consistent with the notion that *lncFAO* contributes to the resolution of inflammation. *lncFAO* acts by binding to HADHB and enhancing FAO, which is important for the late suppression of cytokine expression. These findings demonstrate that *lncFAO* is a mediator of late metabolic reprogramming of inflammatory macrophages that promotes the resolution of inflammation.

Functional transition of macrophage phenotypes from proinflammatory to proresolution/healing is vital for healing and restoration of homeostasis after tissue injury (3). Interestingly, down-regulation of genes associated with glycolysis and up-regulation of those associated with OXPHOS and FAO precedes the phenotypic transition of macrophages in a muscle injury model (38). In addition, IL-10, which contributes to this phenotypic transition after muscle injury (50), inhibits LPS-induced activation of glycolysis and promotes OXPHOS in BMDMs (51). These reports support the notion that activation of OXPHOS is integral to the macrophage functional transition

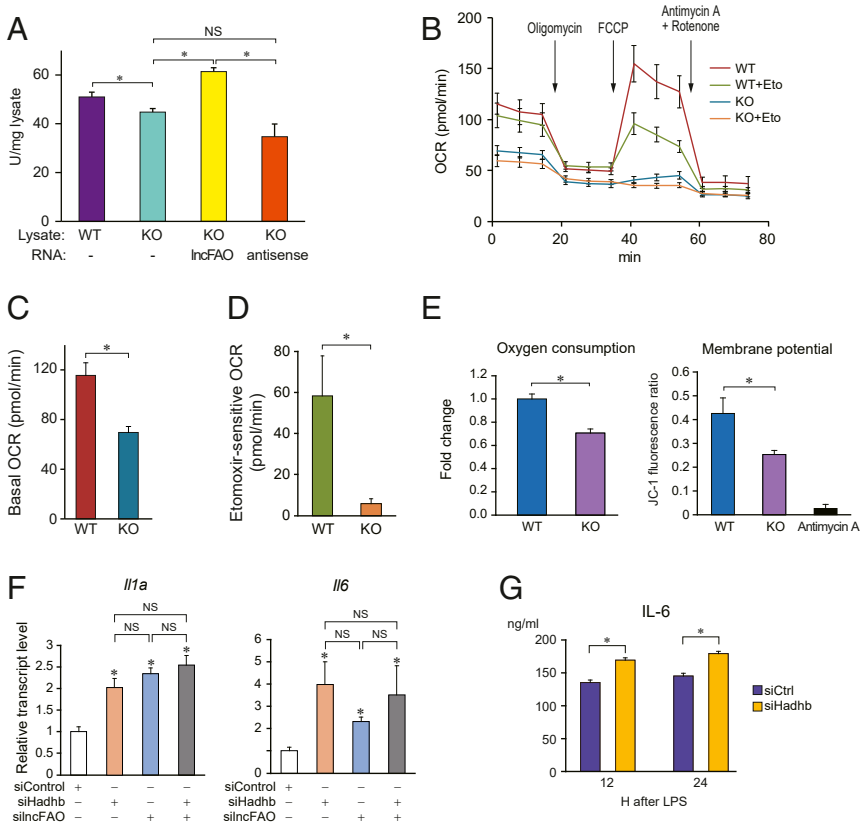


**Fig. 4.** *lncFAO* modulates cellular metabolism. (*A*) Comparison of thiolase activity in lysates of untreated WT and *lncFAO*$^{-/-}$ (KO) BMDMs. In vitro transcribed *lncFAO* or its antisense RNA were added to *lncFAO*$^{-/-}$ lysates, as indicated. The *y* axis indicates the enzyme activity in the cell lysate that converts acetoacetyl-CoA to acetyl-CoA. One unit of activity is defined as the amount of enzyme that converts 1 μmol of acetoacetyl-CoA per minute. **P* < 0.05, Tukey–Kramer's post hoc test. (*B*) Changes in the OCR in WT and *lncFAO*$^{-/-}$ BMDMs treated sequentially with oligomycin (1 μM), FCCP (1.5 μM), and rotenone (0.5 μM) plus antimycin A (0.5 μM) in the presence of BSA and palmitate, with or without pretreatment with 40 μM etomoxir (Eto), an FAO inhibitor, as indicated. (*C*) OCR in untreated BMDMs. *n* = 6. **P* < 0.05, two-tailed unpaired Student's *t* test. (*D*) Etomoxir-sensitive fractions of OCR in FCCP-treated cells. *n* = 6. **P* < 0.05, two-tailed unpaired Student's *t* test. (*E*) The extracellular OCR and mitochondrial membrane potential were measured in WT and *lncFAO*$^{-/-}$ BMDMs 24 h after LPS treatment. OCR was measured using a phosphorescent oxygen probe (MitoXpress) (46). As an index of mitochondrial membrane potential, the ratio of the fluorescence intensity of JC-1 aggregates (595 nm) to that of JC-1 monomers (535 nm) is shown (47). The cells were also treated with the OXPHOS inhibitor antimycin A (10 μM) just before the measurement. *n* = 3. **P* < 0.05, two-tailed unpaired Student's *t* test. (*F*) BMDMs were transfected with siRNA targeting *Hadhb*, *lncFAO*, or control siRNA. Twelve hours after transfection, the cells were treated with LPS. Cellular mRNA levels were analyzed using qPCR 12 after LPS treatment. mRNA levels were first normalized to those of 18s rRNA and then to the level in siCtrl-transfected BMDMs. *n* = 3. *Hadhb* levels are shown in *SI Appendix*, Fig. S10. **P* < 0.05, two-tailed unpaired Student's *t* test. (*G*) BMDMs were transfected with siRNA targeting *Hadhb* or control siRNA. Twenty-four hours after transfection, the cells were treated with LPS. IL-6 levels in the medium were analyzed 12 and 24 h after LPS treatment. *n* = 3. **P* < 0.05, two-tailed unpaired Student's *t* test.

in inflammation. Our present results demonstrate that *lncFAO* is an important regulator of the late changes in macrophage function and FAO during inflammatory responses in BMDMs. Deletion of *lncFAO* down-regulated the genes reflecting the change of Ly6C$^{hi}$ macrophages from the inflammatory to the reparative phase after MI or skeletal muscle injury in BMDMs, which suggests *lncFAO* is important for those changes (Fig. 2*E*). Consistent with those findings, *lncFAO* expression was increased in Ly6C$^{hi}$ macrophages during the repair phase after MI (e.g., ~7 d post-MI), a time when the inflammation seen earlier (e.g., on day 2) was being resolved and reparative processes were progressing (Fig. 1*D* and *SI Appendix*, Figs. S2 and S3). On day 7 post-MI, *lncFAO*-expressing cells also expressed genes related to inflammatory resolution and wound healing, such as *Tgfb1* (*SI Appendix*, Fig. S3). These findings suggest that *lncFAO* is a mediator of the metabolic reprograming required for induction of proresolution functionality in macrophages during inflammation.

We found that *lncFAO* interacts with HADHB. An earlier study reported that HADHB also binds to the 3′UTR of human *REN* mRNA, which decreases the stability of the mRNA (45). Although to our knowledge this report of an RNA affecting HADHB activity is unique, several proteins have been shown to interact with HADHB and modulate its activity (52, 53). For example, estrogen receptor α (ERα) interacts with HADHB within mitochondria and modulates its thiolase activity (52). This interaction may mediate estrogen-induced alterations in lipid metabolism. HADHB may also interact with other proteins and RNAs, enabling it to act as a hub enzyme that controls metabolism in response to multiple inputs.

Recent studies have identified RNA-binding activities in many metabolic enzymes, some of which affect the fate of the bound RNAs (54). For exampl, glyceraldehyde 3-phosphate dehydrogenase (GAPDH) reduces translation of *TNF* mRNA in monocytes by binding to its 3′UTR (55). Moreover, the glycolysis rate is a key determinant of GAPDH binding to *TNF* mRNA, suggesting that GAPDH links the cellular metabolic state to cytokine production. Similarly, GAPDH binds to the 3′UTR of *Ifng* mRNA and suppresses its translation in effector T cells (56). Those findings and our present results highlight the notion that

RNA-binding metabolic enzymes comprise the critical machinery that connects cellular metabolism to immune cell activation.

But while it appears that enzymes can affect the fate of RNAs through binding, the effects of RNA binding on enzymatic activity is less clear. We show here that interaction with *lncFAO* activates HADHB enzymatic activity (Fig. 4*A*) and positively regulates mitochondrial HADHB levels (Fig. 3*E*). Our results further demonstrate that RNA-binding enzymes can be regulated by specific RNAs. lncRNAs may also control cellular metabolism via multiple modes of action. For example, *Tug1* controls mitochondrial bioenergetics by activating proliferator-activated receptor γ coactivator α (PGC-1α) in podocytes (57). *SAMMSON* interacts with p32, a critical regulator of tumor mitochondrial metabolism, and enhances its mitochondrial localization and function in melanoma cells (58). Because expression of lncRNAs is more highly cell-type–selective than expression of mRNAs (25, 59), lncRNAs may have important context-dependent regulatory functions in cellular metabolism. Future studies will need to further address this key biological function of lncRNAs.

## Methods

**Mice.** C57BL/6J mice were purchased from Japan Clea. *lncFAO* knockout mice were created using CRISPR-Cas9 technology (60). A mixture of in vitro-transcribed Cas9 mRNA and two types of single-guide RNA (sgRNA) were injected into fertilized eggs of C57BL/6J mice. To construct plasmids encoding each sgRNA, annealed oligonucleotides were inserted into a pDR274 vector digested with BsaI (61). The genomic target DNA sites and the sequences of the annealed oligonucleotides were as follows: sgRNA#1, 5′-AGC CTAACACAATGGGTGAGGGG-3′; sgRNA#2, 5′-GTAGCAGAGAGTTGTACGTCT GG-3′. These sequences were designed by CRISPR Design (https://zlab.bio/guide-design-resources).

To analyze deletion of the target region, genomic PCR was conducted using the primers 5′-GGGGAGAACCTGCTAGAAGC-3′ and 5′-GAGGTCTTATTC TTTCCAGAACACTG-3′. We generated five lines of mice, each with different types of deletions. By sequencing the genomic DNA of the vicinity of the guide RNA target sites, we found that two lines had an allele with a >200-bp deletion at the first exon of *lncFAO* and further characterized those lines.

To assess possible off-target deletions, off target candidate sites were identified using CRISPR Design tools and amplified from genomic DNA extracted from the tails of mice in the two lines. The target site was also amplified as a positive control. PCR products from WT and knockout mice were mixed, and DNA hybridization was performed as follows: Initial heating at 95 °C for 5 min, followed by gradually cooling to 4 °C at 2 °C/min. After hybridization, the mixture was treated with Guide-it Resolvase (Takara), which cuts DNA at mismatches. The primer sequences used for detection of off-target mutations were as follows: Off-target #1, GGCTGC ACTCTGGGCATTAT and TCCGTGCAGACATGAACAGT; off-target #2, GGT AGTCTGGAAAGGGCAGTC and CCTCGTGACACGGATGGTTC; off-target #3, CTTCCACTCAACCACAAGCG and ACCACAGGATCGTTCCCTAA.

We generated mice homozygous for the targeted alleles in the two lines. Mice in the two lines did not show gross anatomical abnormalities and grew normally (*SI Appendix*, Fig. S2*D*). BMDMs prepared from the two lines showed similarly enhanced proinflammatory cytokine gene expression after LPS treatment (*SI Appendix*, Fig. S4*F*). We mainly used the first line (KO1) carrying a 201-bp deletion in the *lncFAO* gene for characterization of *lncFAO* (*SI Appendix*, Fig. S2*A*).

All experiments were approved by the University of Tokyo Ethics Committee for Animal Experiments and strictly adhered to the guidelines for animal experiments of the University of Tokyo.

**Reagents and Antibodies.** For chromatin immunoprecipitation sequencing (ChIP-seq), anti-H3K4me3 (39159; Active motif), anti-PU.1 (sc-352; Santa Cruz), and anti-p65 (sc-372; Santa Cruz) antibodies were used. For Western blotting, anti-HADHB (sc-134922, Santa Cruz; 1:200), anti–α-tubulin (T6199, Sigma Aldrich; 1:2,000), anti-histone H3 (4620, Cell Signaling Technology; 1:2,000), and anti-COX IV (11967, Cell Signaling Technology; 1:1,000) antibodies were used. As secondary antibodies, horseradish peroxidase (HRP)-linked anti-rabbit IgG and anti-mouse IgG (Cell Signaling Technology; 1:2,000) were used. For immunofluorescent staining, anti-COX IV (11967, Cell Signaling Technology; 1:100), anti-HADHB (sc271495, Santa Cruz; 1:50), and anti-p65 (sc-8008, Santa Cruz; 1:50) antibodies were used as primary antibodies. As secondary antibodies, anti-mouse IgG, Alexa Fluor 647 (A-21235, Thermo Fisher; 1:200), and anti-rabbit IgG, Alexa Fluor 488 (A-11034, Thermo Fisher; 1:100) antibodies were used. For flow cytometry, anti-CD11b BV421 (101251, BioLegend), anti–F4/80-PE (123110, BioLegend), anti–Ly6c-PE-Cy7 (128018, BioLegend) and anti–Ly6g-PerCP/Cy5.5 (127615, BioLegend) antibodies were used.

**BMDMs.** All cultures were maintained at 37 °C in a 5% $CO_2$ water-jacketed incubator. Bone marrow cells were flushed from femurs and tibias of male mice between 6 and 9 wk of age, and were grown in DMEM/F12 (Thermo Fisher) supplemented with 10% FBS (HyClone), 1% penicillin–streptomycin (Thermo Fisher), 1% l-glutamine (Thermo Fisher), and 40 ng/mL of recombinant mouse M-CSF (576406; BioLegend) for 7 to 8 d. The medium was changed every 3 d. Differentiated BMDMs were detached from plates using StemPro Accutase Cell Dissociation Reagent (Thermo Fisher) and replated into 12-well tissue culture dishes at a density of $5 \times 10^5$ cells per well prior to cell stimulation. For LPS and Kdo2 lipid A (KLA) treatment, 100 ng/mL of LPS (Sigma-Aldrich) or KLA (Avanti polar lipids) was added to the medium. We found that LPS and KLA increased *lncFAO* transcription and induced histone modifications similarly (Fig. 1*C*). For Fig. 1*C*, data from LPS-treated cells (RNA-seq and ChIP-seq for H3K4me3 and PU.1) and KLA-treated cells (ChIP-seq for H3K27ac and p65) were assembled.

**Wound-Healing Models.** Wound-healing assays were conducted 8 wk after bone marrow transplantation. Under anesthesia, a 6-mm disposable biopsy punch (Kai Medical) was used to generate two wounds in the dorsal skin of each animal (62). Close-up photos of the wounds were taken, and the sizes of the wounds were analyzed using Adobe Photoshop and normalized to a neighboring 6-mm circle seal (*SI Appendix*, Fig. S6*A*). After macroscopic analyses, the more rostral wounds were dissected for flow cytometric analyses, while the more caudal ones were used for pathological assessment.

**Flow Cytometry.** Samples for flow cytometry were prepared as previously described (63). Briefly, mice were anesthetized and the heart was exposed and perfused with 10 mL PBS from the left ventricle. Thereafter, the whole heart tissue was excised, and the right and left atria and atrioventricular valves were removed. The excised biventricles were mechanically minced using a scalpel. The tissue was then incubated in DMEM containing 1% elastase (Worthington Biochemical) for 120 min at 37 °C. During the incubation, the cells in the suspension were dissociated by sequentially passing the extract through 20-, 21-, and 23-gauge needles at 30-min intervals. The cells were further dissociated by passing them through a 23-gauge needle three times and filtered through a 40-μm cell strainer (BD). The cells were then centrifuged at $300 \times g$ for 5 min, washed with PBS, and resuspended in FACS buffer (PBS supplemented with 1% FBS). After removing erythrocytes by using BD PharmLyse solution (BD), isolated cells were stained with fluorochrome-conjugated antibody.

Skin macrophages within the wound were isolated as described previously (64). The excised skin, without the excess fat, was immersed for 30 min at 37 °C in HBSS, which lacked calcium and magnesium and contained 5 mM EDTA, 10 mM Hepes, and 10% FBS. The skin fragments were then cut into small pieces with a scissors and immersed for 30 min at 37 °C in the HBSS. After washing, the skin pieces collected using a 70-μm strainer (BD) were incubated for 30 min at 37 °C in the HBSS supplemented with 0.7 mg/mL collagenase D. The isolated cells from the digested skins were filtered through a 40-μm cell strainer and resuspended in FACS buffer. After removing erythrocytes with BD PharmLyse solution (BD), cells were stained with fluorochrome-conjugated antibody as above.

**Segmentation of Cellular Compartments.** Cytosolic and nuclear compartments were isolated using a PARIS Kit (Thermo Fisher). RNA from each fraction was eluted in an equal amount of water, and equal volumes of RNA lysate were used for RT-PCR. The nuclear, mitochondrial, and cytosolic fractions were isolated using a Cell Fractionation Kit (ab109719, Abcam).

**Purification of RNA and Real-Time PCR.** Total RNA was purified from cells and tissues by using RNeasy and RNeasy plus micro RNA Purification kits (Qiagen), respectively, according to the manufacturer's instructions. Prior to RNA sequencing, the cell lysates were passed through a gDNA Eliminator spin column to eliminate potential contamination by genomic DNA. Total RNA was converted to cDNA using SuperScript III (Thermo Fisher). Quantitative real-time PCR analyses were carried out using a Lightcycler 480 system (Roche), with 18S rRNA serving as an internal control. The sequences of the primers used are as follows: *18S*, 5′-AAACGGCTACCACATCCAAG-3′ and 5′-CGCTCCCAAGATCCAACTAC-3′; *lncFAO*, 5′-TGCTACCTCCTCGGTGCTAC-3′ and 5′-TGTTGCTAGGCACTGGAAAA-3′; *Il1a*, 5′-TTGGTTAAATGACCTGCAACA-3′

and 5′-GAGCGCTCACGAACAGTTG-3′; *Il1b*, 5′-TGTAATGAAAGACGGCACACC-3′ and 5′-TCTTCTTTGGGTATTGCTTGG-3′; *Il6*, 5′-GCTACCAAACTGGATATAATCAGGA-3′ and 5′-CCAGGTAGCTATGGTACTCCAGAA-3′; *S100a8*, 5′-TCCTTGCGATGGTGATAAAA-3′ and 5′-GGCCAGAAGCTCTGCTACTC-3′; *Hadhb*, 5′-GATGGAGGCCAGTATGCTTT-3′ and 5′-AGTCGGTCGCCTCCTTCTA-3′.

***lncFAO* and *Hadhb* Knockdown.** Cells were transfected with siRNAs using Lipofectamine RNAiMax (Thermo Fisher) according to the manufacturer's instructions. Reverse transfection was performed by adding medium and detached BMDMs to prepared siRNA and lipid complexes inside wells. Stealth RNAi siRNA Negative Control Lo GC Duplex #2 (Thermo Fisher) served as a negative control. Predesigned Stealth RNAi siRNAs for *Hadhb* knockdown were purchased from Thermo Fisher Scientific. The sequences of two types of *silncFAO* were designed using BLOCK-iT RNAi Designer (https://rnaidesigner.thermofisher.com/rnaiexpress/). The sequences of the siRNAs were as follows: siIncFAO#1, 5′-CAAGAGAGAAAGUACUGUUUGGGUA-3′ (sense) and 5′-UACCCAAACAGUACUUUCUCUCUUG-3′ antisense; siIncFAO#2, 5′-AGGGAUCAGUUUAGCAGCCUAGAUA-3′ (sense) and 5′-UAUCUAGGCUGCUAAACUGAUCCCU-3′ (antisense); siHADHB, 5′-GGAUCACCUCCUCUGGAGAAGUUUA-3′ (sense) and 5′-UAAACUUCUCCAGAGGAGGUGAUCC-3′ (antisense).

***lncFAO* Overexpression.** A full-length *lncFAO* cDNA was amplified from cDNA from LPS-treated BMDMs. The primer sequences used with PCR for cloning were 5′-gtcgacGCCATCCAGACGTACAACTCTCT-3′ and 5′-gcggccgcAGGAAAGAGTTTATTTGGAGCTTACATTTTC-3′. The cDNA was cloned into pGEM-T Easy Vector (Promega) and then the *lncFAO* insert was sublconed into pcDNA3.1(+) vector (Thermo Fisher). A mixture of 1 μg of the expression vector and 3 μL of lipofectamine 2000 (Thermo Fisher) was added to the medium in each well of a 12-well culture plate, after which $5 \times 10^5$ cells were added to each well. As a control the empty vector was transfected. Twenty-four hours after transfection the cell were treated with LPS.

**Western Blotting.** Samples of protein lysate supplemented with 1× cOmplete proteinase inhibitor mixture (Sigma-Aldrich) and loading buffer were boiled, after which the proteins were separated by SDS/PAGE, transferred to a nitrocellulose blotting membrane (GE Healthcare), blocked with 5% skim milk, and incubated with primary antibodies at 4 °C overnight. Proteins were visualized using HRP-linked secondary antibody and ECL Prime (GE Healthcare) and then captured using ImageQuant LAS 4000 (GE Healthcare). The same membrane was then stripped using Stripping solution (Wako) and sequentially incubated with other primary antibodies, as multiple proteins were targeted.

**FISH and Immunofluorescent Staining.** BMDMs were seeded into eight-well chamber slides at a density of $10^5$ cells per well, fixed with 10% neutral buffered formalin at room temperature for 30 min, dehydrated with ethanol, and stored at −20 °C. RNA FISH was performed using a RNAscope 2.5 HD Reagent Kit-RED (Advance Cell Diagnostics) according to the manufacturer's protocol. Briefly, the fixed cells were rehydrated followed by treatment with hydrogen peroxide and protease III. The sample was hybridized with probes designed for *lncFAO* by the manufacturer for 2 h at 40 °C, after which the remainder of the assay protocol was implemented.

For immunofluorescent staining, the samples were washed with PBS, blocked by 2% BSA for 30 min, and incubated with a primary antibody against COX-IV and then the secondary antibody for 1 h each at room temperature. After washing the samples with PBS, nuclei were counterstained with DAPI Fluoromount-G (SouthernBiotech). The fluorescent signals were visualized and captured using a confocal laser scanning microscope (LSM510 Meta, Zeiss)

**Analysis of *lncFAO*-Binding Proteins.** To identify *lncFAO* binding proteins, RNA pull-down assays were performed using biotinylated *lncFAO* RNA probe as described previously (41, 65). The plasmid carrying the *lncFAO* cDNA was linearized using NotI and used as the template of in vitro transcription. Biotinylated *lncFAO* RNA was generated using T7 RNA polymerase (Promega) and Biotin RNA labeling mix (Sigma Aldrich). As a control, an antisense *lncFAO* RNA probe was also generated. The in vitro transcribed RNA was treated with RNase-free DNase I and purified using a RNeasy mini kit (Qiagen). RNA was denatured at 60 °C for 10 min and the cooled down to 4 °C before adding it to cell lysates for RNA pull-down.

After treating $10^8$ BMDMs with or without LPS for 24 h, the cytosolic fraction was purified from the cells using a PARIS Kit (Thermo Fisher) and then were diluted to 1 mL with buffer A (150 mM KCl, 25 mM Tris·HCl pH 7.4, 5 mM EDTA, 0.5 mM DTT, 0.5% Nonidet P-40) supplemented with 1× cOmplete protease inhibitor mixture (Sigma Aldrich) and 100 U/mL SUPERase In (Thermo Fisher). The resultant solution was divided into three samples and incubated for 1 h at 4 °C with 20 μg of biotinylated RNAs, followed by incubation for 45 min with 60 μL of Dynabeads M280 and T1 (Thermo Fisher). A mixture of different size beads was used to increase sedimentation efficacy (66). After incubation, the beads were washed five times with buffer A and boiled with SDS loading buffer. The eluted samples were loaded into 4 to 15% Mini-PROTEAN Precast Gels (Bio-Rad), which was followed by silver staining using a Silver Stain kit (APRO science). The extracted gel band was submitted to APRO science for LC-MS/MS analysis.

**Pull-Down of Endogenous *lncFAO*-Containing Complexes.** To pull down proteins associated with *lncFAO*, we modified the procedures used for the ChIRP method (43, 44). The original ChIRP protocol was developed to isolate genomic regions bound by an RNA of interest. We modified that protocol to obtain proteins that associate with *lncFAO* RNA within cells. Endogenous RNA–protein complexes were retrieved using 10 biotinylated oligonucleotides corresponding to the complementary sequence of *lncFAO*. Briefly, 24 h after LPS treatment, BMDMs were fixed with 3% formaldehyde for 30 min at room temperature, quenched in 0.125 M glycine for 5 min, and snap frozen. For experimentation, the cell pellets were thawed in a 10× volume of lysis buffer (50 mM Tris·HCl pH 7.0, 10 mM EDTA, 1% SDS, supplemented with cOmplete and 0.2 U/mL SUPERase-In) and sonicated for 8 min using a Covaris S220. The resultant lysates were diluted with two volumes of hybridization buffer (750 mM NaCl, 1% SDS, 50 mM Tris·HCl 7.0, 1 mM EDTA, 15% Formamide, cOmplete and SUPERase-In) and divided into three equal aliquots. The aliquots were incubated first with 50 pmol/mL biotinylated anti-*lncFAO* oligos or anti-LacZ oligos, or with 10 μg/mL RNase A (Sigma Aldrich) at 37 °C overnight. This was followed by incubation for an additional 30 min with 100 μL/mL Dynabeads MyOne Streptavidin C1 (Thermo Fisher). After the incubations, the beads were washed five times with wash buffer (1× SSC, 0.5% SDS, and cOmplete) and incubated in biotin elution buffer (12.5 mM biotin, 7.5 mM Hepes pH 7.5, 75 mM NaCl, 1.5 mM EDTA, 0.15% SDS, 0.075% sarkosyl, and 0.02% Na-Deoxycholate) for 20 min at room temperature and then at 65 °C for 10 min. For protein elution, the eluent was mixed with a 25% total volume of trichloroacetic acid, and the proteins were precipitated at 4 °C overnight. Ten types of anti-*lncFAO* and four types of anti-LacZ 20-mer oligos were designed using online tools available at (https://www.biosearchtech.com/stellaris). Oligos modified with 3′ biotin-TEG were purchased from Eurofins Genomics. For pull-down, a mixture of oligos were used. The sequences of oligos against lncFAO were as follows: AGTATCACCATAGGAGCTTT, CCAGGTAAGGTGATACATCT, ATGTCTGAGTGTATCTAGGC, CTGGCTGGAATCTATAGTCT, CATTCCTCTTTACCTTTCAA, GCTGTGTGTTTATTCTCTTT, GTGAGCTCAGACTGTAGATT, TCAAGATGCATTATCTGCGC, GGACTCATGACTCTTCTTTC, CTTGACTGATGTGATGTTCC. The sequences of oligos against LacZ were described previously (43).

**Cytokine ELISA.** Culture media from BMDMs in 12-well plates were harvested and centrifuged at 700 × *g* to remove debris. ELISAs were then performed following the instructions provided with BioLegend's ELISA MAX kits (mouse IL-1α: 433401, IL-1β: 432601, and IL-6: 431301). Cytokine concentrations were calculated based on the subtraction of absorbance at 570 nm from that at 450 nm. Absorbances were measured using an EnSpire plate reader (PerkinElmer).

**RNA Sequencing.** Poly-A mRNA was extracted from total RNA by using an Oligo-dT beads of TruSeq RNA Sample Prep Kit v2 (Illumina) or Oligo-dT beads of NEBNext Poly(A) RNA Magneic Isolation Module (New England Biolabs), after which RNA-seq libraries were prepared using a ScriptSeq v2 RNA-Seq Library Preparation Kit (Epicentre) or NEBNext Ultra II RNA Library Prep Kit for Illumina (New England Biolabs) according to the manufacturers' protocols. Libraries were single-end–sequenced or paired-end–sequenced on GAIIx or HiSEq. 1500 sequencer (Illumina). Reads were aligned to the mm9 or mm10 mouse genome using Bowtie (66) and TopHat (67) or STAR (68). Aligned read files were analyzed using Cufflinks (69) and HOMER (70). Cufflinks identified gene loci of novel lncRNAs, including *lncFAO*, from the reads of RNA-seq, and the 5′ end of *lncFAO* was confirmed with reference to CAGE data from FANTOM (https://fantom.gsc.riken.jp/zenbu/). Expression analysis of the RNA-seq data were performed using HOMER and Genomatix. Gene set enrichment was performed using GSEA (28) with rank files generated as previously described (71) from expression data analyzed using DESeq2 (72, 73).

**ChIP Sequencing.** ChIP assays were performed as described previously (74). After BMDMs were cross-linked with 1% formaldehyde for 10 min at room temperature and quenched with 0.25 M glycine, cell pellets were lysed in SDS lysis buffer (1% SDS, 10 mM EDTA, 50 mM Tris·HCl pH 8.1, supplemented with cOmplete). Chromatin was sheared to 250-bp to 400-bp fragments

using a Covaris S220 μLtrasonicator, diluted 10× in ChIP dilution buffer (0.01% SDS, 1.1% Triton X-100, 1.2 mM EDTA, 16 mM Tris·HCl pH 8.1, 167 mM NaCl), and incubated with 1 μg of primary antibodies at 4 °C overnight. The protein–DNA complexes immunoprecipitated with Dynabeads Protein A or G (Thermo Fisher) were washed twice with low-salt wash buffer (0.1% SDS, 1% Triton X-100, 2 mM EDTA, 20 mM Tris·HCl pH 8.1, 150 mM NaCl), twice with high-salt wash buffer (0.1% SDS, 1% Triton X-100, 2 mM EDTA, 20 mM Tris·HCl pH 8.1, 500 mM NaCl), twice with LiCl buffer (0.25 M LiCl, 0.5% Nonidet P-40, 0.5% Na Deoxycholate, 1 mM EDTA, 10 mM Tris·HCl pH 8.1), and once with TE (10 mM Tris·HCl pH 7.6, 1 mM EDTA). Bound protein–DNA complexes were eluted using elution buffer (1% SDS, 100 mM $Na_2HCO_3$) and reversed by addition of 5 M NaCl overnight at 65 °C. ChIP-seq libraries were prepared using a TruSeq ChIP Library Preparation kit (Illumina) according to the manufacturer's protocol. Libraries were single-end-sequenced on GAIIx or HiSEq. 1500 sequencers (Illumina).

**Single-Cell Transcriptome Analysis.** FASTQ data downloaded from ArrayExpress (E-MTAB-7376) (37) were processed using 10X Genomics Cell Ranger count software. The sequence of *lncFAO* was appended to the mm10 reference. The standard procedures of filtering, log-normalization, and variable gene selection were performed using Seurat v3 (75). We filtered cells that expressed fewer than 200 unique molecular identifiers, and the percentage of counts mapped to the mitochondrial genome was ≥5%. To exclude possible doublets, cells with high unique molecular identifier counts were also removed. Six datasets (sham, day 3 and 7 post-MI of total interstitial cells and *Pdgfra*$^+$ cells) (37) were aggregated using Seurat's standard data integration procedure with 2,000 highly variable genes. The expression matrix was dimensionally reduced using principal component analysis of the corrected integrated gene matrix. Clusters were identified using a graph-based approach with the Louvian modularity optimization algorithm. We employed t-distributed stochastic neighbor embedding for dimensionality reduction and visualization of our datasets. For visualization of gene expression, the MAGIC algorism was used to impute drop-out values (76).

We first analyzed expression of *lncFAO* in the total dataset (*SI Appendix*, Fig. S2*A*). Most of the cells expressing *lncFAO* were found in the clusters expressing *Ptprc*, *Itgam*, and *Cd68*. We then analyzed a subset of clusters expressing *Ptprc* and *Cd68*, after which the cells were clustered again to further identify subpopulations (*SI Appendix*, Fig. S2 *B* and *C*).

To identify genes differentially expressed between day 3 and day 5 post-MI in a cluster, MAGIC-imputed data were analyzed using Seurat's FindMarkers function with the MAST algorithm (77). Highly expressed genes that had an adjusted $P < 0.001$ and $\log_2$ fold-change $> 0.25$ were selected. The gene sets were used for the GSEA shown in Fig. 2*E*. To identify the signature genes of a cluster on day 7, gene expression was compared with that of the remaining clusters and the more highly expressed genes that had adjusted $P < 0.05$ and $\log_2$ fold-change $> 0.2$ were selected. The gene set enrichment was analyzed using Metascape (78) with the default parameters for *SI Appendix*, Fig. S3*B*. For GSEA (*SI Appendix*, Fig. S3*C*), the results of the MAST test of the genes with $\log_2$ fold-change $> 0.1$ were used to generate rank files.

**Skeletal Muscle Signature Gene Set.** Microarray data analyzed in supplemental table 1 in Varga et al. (38) were used to identify genes enriched in Ly6C$^{hi}$ macrophages on day 4 postinjury in cardiotoxin-injured skeletal muscle. The genes whose expression was significantly higher in Ly6C$^{hi}$ macrophages on day 4 than on day 2 or day 8 were selected from the data and used as the signature genes of Ly6C$^{hi}$ macrophages on day 4 postinjury in Fig. 2*E*.

**Thiolase Activity.** HADHB activity was assessed by monitoring thiolytic cleavage of acetoacetyl-CoA (52, 53). In brief, BMDMs were lysed by sonication in 1 mL of lysis buffer (100 mM Tris·HCl, pH 8.3, 200 mM NaCl, 0.1% hexamethylphosphoric triamide, 2 mM β-mercaptoethanol, 0.5 mM EDTA, 0.5% Tween-20 and protease inhibitor cOmplete) per 100 mg of cell pellets. Cell lysates diluted 10 times in reaction buffer (100 mM Tris·HCl, pH 8.3, 25 mM $MgCl_2$, 100 μM CoA, 40 μM acetoacetyl-CoA) were incubated for 5 min at 30 °C. After the homogenate was centrifuged at 18,000 × *g* for 5 min, the supernatant was used for enzyme assays. Thiolase activity was spectrophotometrically measured by monitoring the absorbance at 303 nm (79). Mixtures of acetoacetyl CoA and CoA at several concentrations in reaction buffer were measured at the same time to construct a standard curve. One unit of activity was defined as the amount of enzyme that converted 1 μmol of acetoacetyl-CoA in 1-min. For each treatment, the enzymatic activity was measured three times.

**Measurement of Energy Metabolism.** The OCR of BMDMs was analyzed using a XF-96 Extracellular Flux Analyzer (Seahorse Bioscience). BMDMs were plated in a 96-well Seahorse plate (40,000 cells per well) and incubated overnight in a complete medium (DMEM/F12 containing L-glutamine, 10% FBS and 40 ng/mL M-CSF). The next day, the medium was changed to FAO assay medium (111 mM NaCl, 4.7 mM KCl, 1.25 mM $CaCl_2$, 2.0 mM $MgSO_4$, 1.2 mM $NaH_2PO_4$, 2.5 mM glucose, 0.5 mM carnitine and 5 mM Hepes) and incubated for 30 min. Then, after a pretreatment with etomoxir (40 μM) for 15 min, palmitate-BSA (200 μM palmitate conjugated with 34 μM BSA) or BSA (34 μM) (Seahorse Bioscience) was added, and the assays were initiated. OCR was obtained as pmol of $O_2$ consumed per minute. At the same time, extracellular acidification rate was measured as a change in pH. The wells were sequentially treated with the ATP synthase inhibitor oligomycin (1.0 μM), the chemical uncoupler FCCP (1.5 μM), and the electron transport inhibitor antimycin A/rotenone (0.5 μM each).

OCR and mitochondrial membrane potential were also measured using MitoXpress Xtra (80) (600880; Cayman) according to the manufacturer's protocol. BMDMs were plated in a 96-well plate at 60,000 cells per well and incubated for 6 h, after which they were treated with 100 ng/mL LPS for 24 h as described above in the section on culture of BMDMs. The following day, the cells were incubated with JC-1 staining solution for 30 min and, after refreshing the medium, MitoXpress Xtra solution was added. The time-resolved fluorescence (excitation 380 nm/emission 650 nm) was measured using an EnSpire multiplate reader at 37 °C for 60 min. Subsequently, fluorescence intensities for JC-1 monomers (excitation 485 nm/emission 535 nm) and JC-1 aggregates (excitation 535 nm/emission 590 nm) were measured.

**Data Availability.** All RNA-seq and ChIP-seq data are available in the Gene Expression Omnibus under accession number GSE130056. Our previous ChIP-seq results used in this study are also available (accession number GSE95712) (81).

**ACKNOWLEDGMENTS.** We thank Drs. Atsushi Okabe, Masaki Fukuyo, and Bahityar Rahmutulla for next-generation sequencing; and M. Hayashi, X. Yingda, N. Yamanaka, M. Hatase, and K. Ogasawara for excellent technical assistance. This study was supported in part by the Grant-in-Aid for Scientific Research 18K08061 (to Y.N.), 17H04171 and 19K22615 (to K.F.), 20H03679 (to Y.O.), and 17KT0047 and 19H03648 (to I.M.); Grant-in-Aid for Scientific Research on Innovative Areas Preventive Medicine through Inflammation Cellular Sociology 20H04956 (to Y.O.), 20H04938 (to I.M.) from the MEXT Japan; JP19ek0310013, JP19jm0210052, and JP19gm6110006 (to K.F.), JP19gm5910021h9903 (to Y.O.), and JP20gm5010002 (to I.M.) from the Japan Agency for Medical Research and Development; Precursory Research for Embryonic Science and Technology JPMJPR13M7 (to K.F.) from Japan Science and Technology Agency; and grants from MSD Life Science Foundation International and the Japan Foundation for Applied Enzymology (to Y.N.), Takeda Science Foundation (to Y.O. and I.M.), and Uehara Memorial Foundation (to I.M.).

1. S. Ghisletti *et al.*, Identification and characterization of enhancers controlling the inflammatory gene expression program in macrophages. *Immunity* **32**, 317–328 (2010).
2. C. K. Glass, G. Natoli, Molecular control of activation and priming in macrophages. *Nat. Immunol.* **17**, 26–33 (2016).
3. Y. Oishi, I. Manabe, Macrophages in inflammation, repair and regeneration. *Int. Immunol.* **30**, 511–528 (2018).
4. M. L. Novak, T. J. Koh, Phenotypic transitions of macrophages orchestrate tissue repair. *Am. J. Pathol.* **183**, 1352–1363 (2013).
5. Y. Oishi, I. Manabe, Macrophages in age-related chronic inflammatory diseases. *NPJ Aging Mech. Dis.* **2**, 16018 (2016).
6. J. Van den Bossche, L. A. O'Neill, D. Menon, Macrophage immunometabolism: Where are we (Going)? *Trends Immunol.* **38**, 395–406 (2017).
7. L. A. J. O'Neill, R. J. Kishton, J. Rathmell, A guide to immunometabolism for immunologists. *Nat. Rev. Immunol.* **16**, 553–565 (2016).
8. M. D. Buck, R. T. Sowell, S. M. Kaech, E. L. Pearce, Metabolic instruction of immunity. *Cell* **169**, 570–586 (2017).
9. M. Guttman *et al.*, lincRNAs act in the circuitry controlling pluripotency and differentiation. *Nature* **477**, 295–300 (2011).
10. S. Loewer *et al.*, Large intergenic non-coding RNA-RoR modulates reprogramming of human induced pluripotent stem cells. *Nat. Genet.* **42**, 1113–1117 (2010).
11. W. Hu, B. Yuan, J. Flygare, H. F. Lodish, Long noncoding RNA-mediated anti-apoptotic activity in murine erythroid terminal differentiation. *Genes Dev.* **25**, 2573–2578 (2011).
12. C. A. Klattenhoff *et al.*, Braveheart, a long noncoding RNA required for cardiovascular lineage commitment. *Cell* **152**, 570–583 (2013).

13. F. Xu, L. Jin, Y. Jin, Z. Nie, H. Zheng, Long noncoding RNAs in autoimmune diseases. *J. Biomed. Mater. Res. A* **107**, 468–475 (2019).
14. S. A. Bhat *et al*., Long non-coding RNAs: Mechanism of action and functional utility. *Noncoding RNA Res.* **1**, 43–50 (2016).
15. Z. Wang, Y. Zheng, lncRNAs regulate innate immune responses and their roles in macrophage polarization. *Mediators Inflamm.* **2018**, 8050956 (2018).
16. S. Carpenter *et al*., A long noncoding RNA mediates both activation and repression of immune response genes. *Science* **341**, 789–792 (2013).
17. M. Krawczyk, B. M. Emerson, p50-associated COX-2 extragenic RNA (PACER) activates COX-2 gene expression by occluding repressive NF-κB complexes. *eLife* **3**, e01776 (2014).
18. Z. Li *et al*., The long noncoding RNA THRIL regulates TNFα expression through its interaction with hnRNPL. *Proc. Natl. Acad. Sci. U.S.A.* **111**, 1002–1007 (2014).
19. J. Chan *et al*., Cutting edge: A natural antisense transcript, AS-IL1α, controls inducible transcription of the proinflammatory cytokine IL-1α. *J. Immunol.* **195**, 1359–1363 (2015).
20. Y. Lu *et al*., The NF-κB-responsive long noncoding RNA FIRRE regulates post-transcriptional regulation of inflammatory gene expression through interacting with hnRNPU. *J. Immunol.* **199**, 3571–3582 (2017).
21. H. Cui *et al*., The human long noncoding RNA lnc-IL7R regulates the inflammatory response. *Eur. J. Immunol.* **44**, 2085–2095 (2014).
22. M. K. Atianand *et al*., A long noncoding RNA lincRNA-EPS acts as a transcriptional brake to restrain inflammation. *Cell* **165**, 1672–1685 (2016).
23. M. Du *et al*., The LPS-inducible lncRNA Mirt2 is a negative regulator of inflammation. *Nat. Commun.* **8**, 2049 (2017).
24. Y. Oishi *et al*., SREBP1 contributes to resolution of pro-inflammatory TLR4 signaling by reprogramming fatty acid metabolism. *Cell Metab.* **25**, 412–427 (2017).
25. T. Derrien *et al*., The GENCODE v7 catalog of human long noncoding RNAs: Analysis of their gene structure, evolution, and expression. *Genome Res.* **22**, 1775–1789 (2012).
26. C. C. Hon *et al*., An atlas of human long non-coding RNAs with accurate 5′ ends. *Nature* **543**, 199–204 (2017).
27. C. Trapnell *et al*., Differential gene and transcript expression analysis of RNA-seq experiments with TopHat and Cufflinks. *Nat. Protoc.* **7**, 562–578 (2012).
28. A. Subramanian *et al*., Gene set enrichment analysis: A knowledge-based approach for interpreting genome-wide expression profiles. *Proc. Natl. Acad. Sci. U.S.A.* **102**, 15545–15550 (2005).
29. A. Liberzon *et al*., The Molecular Signatures Database (MSigDB) hallmark gene set collection. *Cell Syst.* **1**, 417–425 (2015).
30. F. Musacchia, S. Basu, G. Petrosino, M. Salvemini, R. Sanges, Annocript: A flexible pipeline for the annotation of transcriptomes able to identify putative long non-coding RNAs. *Bioinformatics* **31**, 2199–2201 (2015).
31. L. Wang *et al*., CPAT: Coding-Potential Assessment Tool using an alignment-free logistic regression model. *Nucleic Acids Res.* **41**, e74 (2013).
32. A. Barski *et al*., High-resolution profiling of histone methylations in the human genome. *Cell* **129**, 823–837 (2007).
33. S. Heinz, C. E. Romanoski, C. Benner, C. K. Glass, The selection and function of cell type-specific enhancers. *Nat. Rev. Mol. Cell Biol.* **16**, 144–154 (2015).
34. A. S. Nord *et al*., Rapid and pervasive changes in genome-wide enhancer usage during mammalian development. *Cell* **155**, 1521–1531 (2013).
35. I. Hilgendorf *et al*., Ly-6Chigh monocytes depend on Nr4a1 to balance both inflammatory and reparative phases in the infarcted myocardium. *Circ. Res.* **114**, 1611–1622 (2014).
36. M. L. Lindsey, J. J. Saucerman, K. Y. DeLeon-Pennell, Knowledge gaps to understanding cardiac macrophage polarization following myocardial infarction. *Biochim. Biophys. Acta* **1862**, 2288–2292 (2016).
37. N. Farbehi *et al*., Single-cell expression profiling reveals dynamic flux of cardiac stromal, vascular and immune cells in health and injury. *eLife* **8**, e43882 (2019).
38. T. Varga *et al*., Highly dynamic transcriptional signature of distinct macrophage subsets during sterile inflammation, resolution, and tissue repair. *J. Immunol.* **196**, 4771–4782 (2016).
39. A. Kimball *et al*., Ly6C$^{Hi}$ blood monocyte/macrophage drive chronic inflammation and impair wound healing in diabetes mellitus. *Arterioscler. Thromb. Vasc. Biol.* **38**, 1102–1114 (2018).
40. J. Zhao, B. K. Sun, J. A. Erwin, J. J. Song, J. T. Lee, Polycomb proteins targeted by a short repeat RNA to the mouse X chromosome. *Science* **322**, 750–756 (2008).
41. J. L. Rinn *et al*., Functional demarcation of active and silent chromatin domains in human HOX loci by noncoding RNAs. *Cell* **129**, 1311–1323 (2007).
42. K. L. Yap *et al*., Molecular interplay of the noncoding RNA ANRIL and methylated histone H3 lysine 27 by polycomb CBX7 in transcriptional silencing of INK4a. *Mol. Cell* **38**, 662–674 (2010).
43. C. Chu, K. Qu, F. L. Zhong, S. E. Artandi, H. Y. Chang, Genomic maps of long noncoding RNA occupancy reveal principles of RNA-chromatin interactions. *Mol. Cell* **44**, 667–678 (2011).
44. C. Chu *et al*., Systematic discovery of Xist RNA binding proteins. *Cell* **161**, 404–416 (2015).
45. D. J. Adams *et al*., HADHB, HuR, and CP1 bind to the distal 3′-untranslated region of human renin mRNA and differentially modulate renin expression. *J. Biol. Chem.* **278**, 44894–44903 (2003).
46. M. Buler, S.-M. Aatsinki, V. Izzi, J. Uusimaa, J. Hakkola, SIRT5 is under the control of PGC-1α and AMPK and is involved in regulation of mitochondrial energy metabolism. *FASEB J.* **28**, 3225–3237 (2014).
47. B. Kumar, S. Koul, L. Khandrika, R. B. Meacham, H. K. Koul, Oxidative stress is inherent in prostate cancer cells and is required for aggressive phenotype. *Cancer Res.* **68**, 1777–1785 (2008).
48. P.-S. Liu *et al*., α-ketoglutarate orchestrates macrophage activation through metabolic and epigenetic reprogramming. *Nat. Immunol.* **18**, 985–994 (2017).
49. L. S. Pike, A. L. Smift, N. J. Croteau, D. A. Ferrick, M. Wu, Inhibition of fatty acid oxidation by etomoxir impairs NADPH production and increases reactive oxygen species resulting in ATP depletion and cell death in human glioblastoma cells. *Biochim. Biophys. Acta* **1807**, 726–734 (2011).
50. B. Deng, M. Wehling-Henricks, S. A. Villalta, Y. Wang, J. G. Tidball, IL-10 triggers changes in macrophage phenotype that promote muscle growth and regeneration. *J. Immunol.* **189**, 3669–3680 (2012).
51. W. K. E. Ip, N. Hoshi, D. S. Shouval, S. Snapper, R. Medzhitov, Anti-inflammatory effect of IL-10 mediated by metabolic reprogramming of macrophages. *Science* **356**, 513–519 (2017).
52. Z. Zhou, J. Zhou, Y. Du, Estrogen receptor alpha interacts with mitochondrial protein HADHB and affects beta-oxidation activity. *Mol. Cell Proteomics* **11**, M111.011056 (2012).
53. Y.-T. Kao *et al*., Japanese encephalitis virus nonstructural protein NS5 interacts with mitochondrial trifunctional protein and impairs fatty acid β-oxidation. *PLoS Pathog.* **11**, e1004750 (2015).
54. A. Castello *et al*., Insights into RNA biology from an atlas of mammalian mRNA-binding proteins. *Cell* **149**, 1393–1406 (2012).
55. P. Millet, V. Vachharajani, L. McPhail, B. Yoza, C. E. McCall, GAPDH binding to TNF-α mRNA contributes to posttranscriptional repression in monocytes: A novel mechanism of communication between inflammation and metabolism. *J. Immunol.* **196**, 2541–2551 (2016).
56. C.-H. Chang *et al*., Posttranscriptional control of T cell effector function by aerobic glycolysis. *Cell* **153**, 1239–1251 (2013).
57. J. Long *et al*., Long noncoding RNA Tug1 regulates mitochondrial bioenergetics in diabetic nephropathy. *J. Clin. Invest.* **126**, 4205–4218 (2016).
58. E. Leucci *et al*., Melanoma addiction to the long non-coding RNA SAMMSON. *Nature* **531**, 518–522 (2016).
59. M. N. Cabili *et al*., Integrative annotation of human large intergenic noncoding RNAs reveals global properties and specific subclasses. *Genes Dev.* **25**, 1915–1927 (2011).
60. H. Yang *et al*., One-step generation of mice carrying reporter and conditional alleles by CRISPR/Cas-mediated genome engineering. *Cell* **154**, 1370–1379 (2013).
61. W. Y. Hwang *et al*., Efficient genome editing in zebrafish using a CRISPR-Cas system. *Nat. Biotechnol.* **31**, 227–229 (2013).
62. D. Z. Eichenfield *et al*., Tissue damage drives co-localization of NF-κB, Smad3, and Nrf2 to direct Rev-erb sensitive wound repair in mouse macrophages. *eLife* **5**, e13024 (2016).
63. K. Fujiu *et al*., A heart-brain-kidney network controls adaptation to cardiac stress through tissue macrophage activation. *Nat. Med.* **23**, 611–622 (2017).
64. C. J. Benck, T. Martinov, B. T. Fife, D. Chatterjea, Isolation of infiltrating leukocytes from mouse skin using enzymatic digest and gradient separation. *J. Vis. Exp.*, e53638 (2016).
65. J. Zhao *et al*., Genome-wide identification of polycomb-associated RNAs by RIP-seq. *Mol. Cell* **40**, 939–953 (2010).
66. B. R. So *et al*., A U1 snRNP-specific assembly pathway reveals the SMN complex as a versatile hub for RNP exchange. *Nat. Struct. Mol. Biol.* **23**, 225–230 (2016).
67. C. Trapnell, L. Pachter, S. L. Salzberg, TopHat: Discovering splice junctions with RNA-seq. *Bioinformatics* **25**, 1105–1111 (2009).
68. A. Dobin *et al*., STAR: Ultrafast universal RNA-seq aligner. *Bioinformatics* **29**, 15–21 (2013).
69. C. Trapnell *et al*., Transcript assembly and quantification by RNA-Seq reveals unannotated transcripts and isoform switching during cell differentiation. *Nat. Biotechnol.* **28**, 511–515 (2010).
70. S. Heinz *et al*., Simple combinations of lineage-determining transcription factors prime cis-regulatory elements required for macrophage and B cell identities. *Mol. Cell* **38**, 576–589 (2010).
71. M. Ziemann, How to generate a rank file from gene expression data. *Genome Spot* (2015). http://genomespot.blogspot.com/2015/01/how-to-generate-rank-file-from-gene.html. Accessed 2 June 2020.
72. M. I. Love, W. Huber, S. Anders, Moderated estimation of fold change and dispersion for RNA-seq data with DESeq2. *Genome Biol.* **15**, 550 (2014).
73. V. K. Mootha *et al*., PGC-1alpha-responsive genes involved in oxidative phosphorylation are coordinately downregulated in human diabetes. *Nat. Genet.* **34**, 267–273 (2003).
74. F. Lai *et al*., Activating RNAs associate with Mediator to enhance chromatin architecture and transcription. *Nature* **494**, 497–501 (2013).
75. T. Stuart *et al*., Comprehensive integration of single-cell data. *Cell* **177**, 1888–1902.e21 (2019).
76. D. van Dijk *et al*., Recovering gene interactions from single-cell data using data diffusion. *Cell* **174**, 716–729.e27 (2018).
77. G. Finak *et al*., MAST: A flexible statistical framework for assessing transcriptional changes and characterizing heterogeneity in single-cell RNA sequencing data. *Genome Biol.* **16**, 278 (2015).
78. Y. Zhou *et al*., Metascape provides a biologist-oriented resource for the analysis of systems-level datasets. *Nat. Commun.* **10**, 1523 (2019).
79. B. Middleton, 3-Ketoacyl-CoA thiolases of mammalian tissues. *Methods Enzymol.* **35**, 128–136 (1975).
80. S. Salvioli, A. Ardizzoni, C. Franceschi, A. Cossarizza, JC-1, but not DiOC6(3) or rhodamine 123, is a reliable fluorescent probe to assess delta psi changes in intact cells: Implications for studies on mitochondrial functionality during apoptosis. *FEBS Lett.* **411**, 77–82 (1997).
81. Y. Oishi *et al*., Bmal1 regulates inflammatory responses in macrophages by modulating enhancer RNA transcription. *Sci. Rep.* **7**, 7086 (2017).